Biochimica et Biophysica Acta 1838 (2014) 1199–1207

Contents lists available at ScienceDirect

Biochimica et Biophysica Acta

journal homepage: www.elsevier.com/locate/bbamem

The high resolution structure of tyrocidine A reveals an amphipathic dimer

Patrick J. Loll *, Elizabeth C. Upton, Virginie Nahoum [1], Nicoleta J. Economou [2], Simon Cocklin

Department of Biochemistry and Molecular Biology, Drexel University College of Medicine, Philadelphia, PA 19102, USA

ARTICLE INFO

Article history:
Received 16 September 2013
Received in revised form 20 January 2014
Accepted 27 January 2014
Available online 11 February 2014

Keywords:
Tyrocidine
Antibiotic
Antibiotic resistance
Antimicrobial peptide

ABSTRACT

Tyrocidine A, one of the first antibiotics ever to be discovered, is a cyclic decapeptide that binds to membranes of target bacteria, disrupting their integrity. It is active against a broad spectrum of Gram-positive organisms, and has recently engendered interest as a potential scaffold for the development of new drugs to combat antibiotic-resistant pathogens. We present here the X-ray crystal structure of tyrocidine A at a resolution of 0.95 Å. The structure reveals that tyrocidine forms an intimate and highly amphipathic homodimer made up of four beta strands that associate into a single, highly curved antiparallel beta sheet. We used surface plasmon resonance and potassium efflux assays to demonstrate that tyrocidine binds tightly to mimetics of bacterial membranes with an apparent dissociation constant (K_D) of 10 μM, and efficiently permeabilizes bacterial cells at concentrations equal to and below the K_D. Using variant forms of tyrocidine in which the fluorescent probe *p*-cyano-phenylalanine had been inserted on either the polar or apolar face of the molecule, we performed fluorescence quenching experiments, using both water-soluble and membrane-embedded quenchers. The quenching results, together with the structure, strongly support a membrane association model in which the convex, apolar face of tyrocidine's beta sheet is oriented toward the membrane interior, while the concave, polar face is presented to the aqueous phase.

1. Introduction

The development of antibiotics represents one of the crowning achievements of 20th century medicine, and has vastly reduced the morbidity and mortality caused by infection during the pre-antibiotic era. However, antibiotic resistance has spread throughout most human pathogens [1], while the number of new antibiotics in the drug development pipeline has dwindled [2]. These developments have precipitated a crisis in the treatment of bacterial infections, and threaten to wipe out many of the advances made during the last century. This situation has sparked interest in new classes of antibiotics, many of which exploit different targets than those used by current drugs.

One interesting class of compounds under investigation includes the cyclic natural products tyrocidine A, gramicidin S, and the streptocidins. These compounds are produced as linear precursors by non-ribosomal peptide synthesis in bacteria, which are then cyclized through the action of thioesterase enzymes. Tyrocidine A was the first such molecule to be discovered, having been isolated from *Bacillus brevis* around 1940 by Dubos [3]; it is a major component of a mixture of antibacterial peptides known as tyrothricin, the first antibiotic to be successfully used for the treatment of human disease [4,5]. At about the same time, gramicidin S was shown to be produced by a different bacterial species (*Aneurinibacillus migulanus*, originally classified as *B. brevis*), and subsequently proved to be of considerable medical utility during the Second World War [6]. More recently, similar compounds (streptocidins) have been found in species of *Streptomyces* [7,8]. All of these molecules are cyclic decapeptides containing both D- and L-amino acids (Fig. 1).

As befits the founding member of this class of antibiotics, many aspects of tyrocidine's biology and chemistry have been studied, including its biosynthesis [9–11], physical behavior [12], mechanism [13–16], and structure–activity relationships [17–24]. Tyrocidine A is bacteriocidal toward a wide range of Gram-positive organisms, accumulating on membranes of target bacteria and disrupting membrane integrity. Because the target of the drug is the lipid bilayer, rather than a specific macromolecule, microorganisms would need to introduce large-scale changes in their cellular membranes in order to circumvent the drug's action. The likelihood of this occurrence is extremely low [25], and indeed no membrane alterations that confer resistance to tyrocidine A or gramicidin S have been described. Other mechanisms of resistance are possible, including increases in the thickness of barrier layers [26–28] and complexation with neutralizing agents [29]; however, such mechanisms do not appear to be widespread. Thus, the low

* Corresponding author at: Department of Biochemistry and Molecular Biology, Drexel University College of Medicine, 245 N. 15th St., MS497, Philadelphia, PA 19102, USA. Tel.: +1 215 762 7706; fax: +1 215 762 4452.
E-mail address: ploll@drexelmed.edu (P.J. Loll).
[1] Present address: Institute of Pharmacology and Structural Biology, 205 route de Narbonne, 31077 Toulouse, France.
[2] Present address: Eshelman School of Pharmacy, University of North Carolina, Chapel Hill, NC 27599, USA.

http://dx.doi.org/10.1016/j.bbamem.2014.01.033
0005-2736/

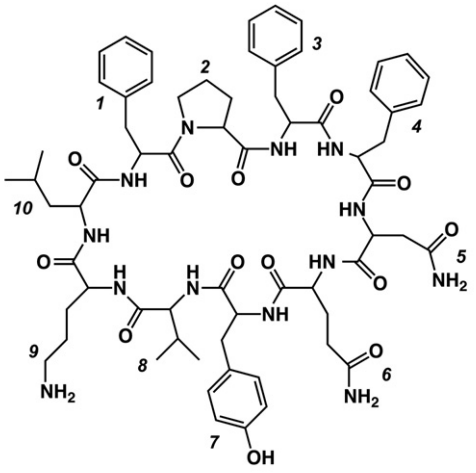

Antibiotic	Sequence
Tyrocidine A	D-Phe-Pro-Phe-D-Phe-Asn-Gln-Tyr-Val-Orn-Leu
Gramicidin S	(D-Phe-Pro-Val-Orn-Leu)$_2$

Fig. 1. Chemical structure of tyrocidine A. The numbering of residues is indicated in the diagram by the italic numerals. Below the figure are shown the sequences of tyrocidine A and the related decapeptide gramicidin S.

probability of eliciting resistance, coupled with the relatively small and simple structure, makes tyrocidine A and related molecules attractive starting points for drug development. In any such development process, selectivity is a critical issue, with drug candidates ideally being highly selective for bacterial membranes over mammalian membranes. Tyrocidine A and gramicidin S are themselves poorly selective; they exhibit considerable hemolytic activity in addition to their antimicrobial effects, which severely limits their therapeutic utility. However, variants have recently been discovered with vastly improved therapeutic indices, displaying both increased antibacterial potency and reduced hemolytic effects [21]. This suggests that it may be feasible to develop this scaffold into a functional therapeutic.

The structure of tyrocidine A has long attracted the attention of scientists; indeed, as long ago as 1955 Dorothy Crowfoot Hodgkin wrote that this molecule's structure is "…of great interest and some importance" [30]. The more recent realization that the tyrocidine scaffold might provide a route to novel therapeutics has only increased interest in high-resolution structural information for tyrocidine, as such information should greatly facilitate the rational interpretation of structure–activity relationship data. Initial progress toward determining the tyrocidine structure came from NMR analyses conducted in the 1980s, which provided the first pictures of tyrocidine [31–34]. However, while these experiments were able to map most of the dihedral angles for the peptide backbone, technical limitations led to ambiguities in certain backbone dihedrals, and also precluded the determination of the conformations of all side chains. Thus, while the NMR work has provided a useful picture of the molecule's overall configuration, many details of the structure have remained unknown.

We present here the first crystal structure for tyrocidine A, determined at a resolution of 0.95 Å. It reveals that the molecule forms an amphipathic dimer, and suggests a model for how the antibiotic interacts with bacterial membranes. We also present functional studies that support this model of membrane interaction.

2. Methods

2.1. Materials

Lipids were purchased from Avanti Polar Lipids (Alabaster, AL, USA). Tyrocidine was synthesized by the method of Bu et al. [35] at Aves Labs (Tigard, OR, USA) and purified by reverse-phase HPLC using a semi-preparative Ultrasphere 5 ODS C18 column (Hichrom, Berkshire, UK). Tyrocidine was eluted with a gradient from 0.1% TFA/100% H_2O to 0.1% TFA/95% acetonitrile; purity was approximately 98%, as estimated from the chromatogram (Fig. S3, Supplementary data). Peak fractions were pooled, lyophilized, and dissolved in methanol at 30 mg/mL. Tyrocidine variants containing *p*-cyanophenylalanine were prepared in the same manner. The crude *p*-cyanophenylalanine variants obtained from the vendor were substantially less pure than the native tyrocidine, complicating their purification. Both purified variants showed a closely-spaced doublet upon re-chromatography on an analytical reverse-phase column, the origin of which is not obvious (Fig. S3, Supplementary data). The doublet was estimated to be 90% pure for [*p*-CN-Phe^4]-tyrocidine and 88% pure for [*p*-CN-Phe^7]-tyrocidine. Masses of the purified antibiotics were verified by mass spectrometry (Drexel University Department of Chemistry and Wistar Institute Proteomics Facility, Philadelphia, PA, USA; Figs. S4 & S5, Supplementary data), and the concentrations of the final tyrocidine solutions were determined using amino acid analysis (Keck Laboratory, Yale University, New Haven, CT, USA).

2.2. Crystallization

Sitting drops containing 10 μL of a tyrocidine solution (30 mg/mL in methanol) were placed on siliconized glass posts (Hampton Research, Aliso Viejo, CA, USA) and equilibrated at 18 °C with a reservoir solution containing a 1:5 (v/v) mixture of 2,4-methylpentanediol (MPD) and methanol. Crystals in the shape of triangular prisms were found after approximately one month. Crystals were mounted on nylon loops, dunked briefly in neat MPD, and flash-cooled in a stream of cold nitrogen gas prior to data collection.

2.3. Crystallographic structure determination and refinement

A single crystal, maintained at 100 K, was used for data collection. Data were measured at beamline X6A of the National Synchrotron Light Source and processed using XDS [36]. Initial structure determination was carried out via direct methods using the SnB program [37]. 78 of the antibiotic's 92 atoms were located after the initial direct-methods phasing; the remaining atoms and solvent molecules were placed in iterative rounds of refinement and map inspection using Coot [38]. The structure was refined using PHENIX v. 1.8.2-1309 [39]. Anisotropic atomic displacement parameters were refined for all non-hydrogen atoms; hydrogen atoms were included for the antibiotic molecule and one ordered MPD solvent molecule, and were refined using a riding model. No hydrogen atoms were included for solvent water or methanol molecules. All of the residues of the antibiotic fall within the most favored region of the Ramachandran diagram. Three methanol molecules were found to lie on or near crystallographic symmetry axes; the largest unmodeled peaks in the final difference Fourier maps are associated with these methanol molecules, and likely reflect the difficulty of adequately modeling disordered solvent lying near symmetry axes. Representative 2Fo–Fc electron density for the final model is shown in Fig. S1 (Supplementary data). Data collection and refinement statistics are given in Table 1. Coordinates and structure factors have been deposited with the Protein Data Bank (PDB ID: 4M6E). Structure figures were made using MacPyMOL (Version 1.5.0.4 Schrödinger, LLC).

2.4. Liposome preparation

Lipids were dissolved in chloroform at 10 mg/mL and mixed in a round-bottom flask in appropriate proportions. The solvent was removed in a rotary evaporator, thereby depositing a thin film of lipid on the walls of the flask. The sample was then moved to a −80° freezer, after which any remaining traces of chloroform were removed by overnight lyophilization. The lipid film was then treated with a buffer

Table 1
Data collection and refinement statistics.

Data collection	
Wavelength (Å)	0.8984
Spacegroup	*R*32 (hexagonal setting)
Cell dimensions (Å)	a = b = 33.39, c = 50.57
Resolution range (Å)[a]	19.0–0.95 (0.97–0.95)
No. observations	84,797 (1654)
No. unique reflections	6973 (454)
Completeness (%)	98.8 (88.5)
Mean multiplicity	12.2 (3.6)
Mean I/σ(I)	48.0 (6.9)
R_{merge}[b]	0.040 (0.161)
R_{meas}[c]	0.041 (0.187)
Refinement	
Resolution range (Å)	19.0–0.95
Number of reflections used	
Working set	6268
Test set	685
Number of antibiotic atoms	92
Number of solvent atoms	
MPD	8
Methanol	6
Water	5
Estimated Wilson B value (Å^2)	9.6
Mean B values (Å^2)	
Antibiotic	8.4
MPD	17.9
Methanol	15.8
Water	12.7
RMS deviations from ideal geometry	
Bond distances (Å)	0.016
Bond angles (deg)	1.80
R_{cryst}/R_{free}	0.134/0.141
Clashscore	0.0

[a] Values in parentheses refer to the highest resolution shell.
[b] R_{merge} is calculated by the equation $R_{merge} = \Sigma_{hkl} \sum_i |I_i(hkl) - \langle I(hkl)\rangle| / \Sigma_{hkl} \sum_i I_i(hkl)$, where $I_i(hkl)$ is the *i*th measurement.
[c] R_{meas} (or redundancy-independent R_{merge}) is calculated by the equation $R_{meas} = \sum_{hkl} [N/(N-1)]^{1/2} \sum_i |I_i(hkl) - \langle I(hkl)\rangle| / \Sigma_{hkl} \sum_i I_i(hkl)$, where $I_i(hkl)$ is the *i*th measurement and *N* is the redundancy of each unique reflection *hkl*.

containing 20 mM HEPES pH 7.0, 100 mM NaF, and 1 mM EDTA. Efficient hydration was achieved by spinning the flask on a rotary evaporator for 2 h (without vacuum), maintaining the temperature between 50 and 60 °C. The flask was then vigorously vortexed for 5 min, after which it was subjected to five freeze–thaw cycles using liquid nitrogen and a 37 °C water bath. The lipid suspension was then passed at least ten times through an Avanti mini-extruder equipped with polycarbonate membranes having 100 nm pores. The size of the resulting liposomes were analyzed by dynamic light scattering using a DynaPro Titan instrument (Wyatt Analytical Technologies, Santa Barbara, CA, USA), yielding an estimated average diameter of 107 nm.

Lipid concentrations were determined by measurements of total phosphorus, following a modification of the method of Chen et al. [40] as described by Avanti Polar Lipids (http://www.avantilipids.com). Briefly, about 0.1 μmol of each liposome preparation was added to the bottom of a glass tube. 450 μL of 4.45 M sulfuric acid were added and the tubes were heated to 210 °C for 25 min. The tubes were then removed from the heating block and allowed to cool for 5 min before adding 150 μL of 30% hydrogen peroxide with vortexing. The samples were then heated above 210 °C for an additional 30 min, and then cooled to room temperature. Next, to each tube was added 3.9 mL of water, 0.5 mL of 2.5% ammonium molybdate(VI), and 0.5 mL of 10% ascorbic acid, with mixing after each addition. Tubes were covered with glass slides to prevent evaporation and heated at 100 °C for 7 min. After cooling to room temperature, the absorbance at 820 nm was measured, using a sample containing no phosphate as the blank. The standard curve was constructed using KH_2PO_4 in 50 mM HCl.

2.5. Surface plasmon resonance

Binding analysis was performed at 25 °C using a Biacore 3000 instrument (GE Life Sciences, Piscataway, NJ, USA). Liposomes were prepared using dipalmitoyl-phosphatidylglycerol, stearamine, and cardiolipin in a 5:1:1 mole ratio, so as to approximately reflect the major phospholipid constituents of *Staphyloccus aureus* membranes [41]. Liposomes were loaded onto the surface of an L1 chip to a density of approximately 1000 response units. Tyrocidine A was injected for a 2 min association phase, followed by a 10 min dissociation phase. Surfaces were regenerated between each injection with CHAPS and the liposomes reloaded to the same density. A blank surface served as the reference. The responses at 100 s (averaged over five separate experiments) were plotted versus tyrocidine A concentration and fit to the four-parameter equation in BiaEvaluation v4.1.1 to obtain the apparent equilibrium dissociation constant (K_D) and its estimated standard deviation.

2.6. Potassium efflux

Leakage of potassium ions from *Micrococcus luteus* cells (ATCC 49732) was measured at 25 °C as described [42], using the potassium-sensitive dye PBFI (Molecular Probes). The EC_{50} value and its associated standard deviation were estimated by fitting a rectangular hyperbola to the equilibrium change in fluorescence as a function of antibiotic concentration.

2.7. Fluorescence quenching experiments

Quenching experiments were conducted using variant forms of tyrocidine in which a D-*p*-cyano-phenylalanine residue was incorporated at position 4 (replacing the native D-Phe), or an L-*p*-cyano-phenylalanine residue was incorporated at position 7 (replacing the native L-Tyr). For all fluorescence experiments a Jobin-Yvon Fluoromax-3 fluorometer was used, exciting at 240 nm and reading emission between 250 and 400 nm. All experiments were conducted at 37 °C. Both tyrocidine variants were used at a concentration of 5 μM in 20 mM HEPES pH 7.0, 100 mM NaF, and 1 mM EDTA.

For experiments using soluble quenchers, liposomes were prepared using a lipid composition of 75 mol% phosphatidylethanolamine, 20 mol% phosphatidylglycerol, and 5 mol% cardiolipin, and used at a final lipid concentration of 660 μM. Quenching was carried out by titrating with KI (concentration range 25 to 300 μM) or acrylamide (concentration range 50 to 600 μM). Fluorescence intensities were corrected for dilution effects.

For experiments using membrane-embedded quenchers, liposomes were prepared using 75 mol% phosphatidylcholine, 20 mol% phosphatidylglycerol, and 5 mol% cardiolipin. Four forms of phosphatidylcholine (PC) were used: 1-palmitoyl-2-oleoyl-PC (unquenched control), 1-palmitoyl-2-(6,7-dibromo)stearoyl-PC, 1-palmitoyl-2-(9,10-dibromo)stearoyl-PC, and 1-palmitoyl-2-(11,12-dibromo)stearoyl-PC. Liposomes were added to tyrocidine solutions to give a final calculated lipid concentration of 1 mM. Fluorescence intensities measured from brominated liposome suspensions were normalized by a factor that scaled the Rayleigh scattering of the suspension to that of the control liposomes. Emission intensities were read at 300 nm ([*p*-CN-Phe^4]-tyrocidine) and 294 nm ([*p*-CN-Phe^7]-tyrocidine).

3. Results

3.1. Structure determination

The crystallization of tyrocidine was reported by Magdoff-Fairchild and White in the late 1970s [43], but no structure followed this report, presumably because of the difficulties associated with phasing such a "large small molecule" structure. In the intervening years, however,

two significant technical advances have occurred, which we reasoned would make tyrocidine's structure determination feasible: bright synchrotron beamlines have become common, improving our ability to measure high-resolution data, and new dual-space direct methods have been introduced that allow facile phase determination for even large molecules [44,45]. In the hopes of applying these advances to the structure determination of tyrocidine, we first produced and optimized well-ordered crystals, using the published crystallization conditions of Magdoff-Fairchild and White as a starting point. As anticipated, when analyzed using modern data collection methods (cryogenic temperatures and an intense synchrotron radiation source), these crystals diffracted strongly, providing data at a resolution in excess of 1 Å (Table 1). This high resolution data set proved highly suitable for structure determination using direct phasing methods, and has yielded a precise model for the antibiotic.

Table 2
Intra- and inter-molecular hydrogen bonds in the tyrocidine dimer.

Donor	Acceptor	Donor–acceptor distance (Å)
Intramolecular		
Phe^3 amide	Leu^{10} carbonyl	3.1
Asn^5 amide	Val^8 carbonyl	2.9
Leu^{10} amide	Phe^3 carbonyl	3.0
Val^8 amide	Asn^5 side chain	2.9
Intermolecular		
D-Phe^1 amide (molecule 1)	Tyr^7 carbonyl (molecule 2)	2.8
Orn^9 amide (molecule 1)	Orn^9 carbonyl (molecule 2)	3.1
D-Phe^1 amide (molecule 2)	Tyr^7 carbonyl (molecule 1)	2.8
Orn^9 amide (molecule 2)	Orn^9 carbonyl (molecule 1)	3.1

3.2. Tyrocidine structure

The tyrocidine molecule forms a two-stranded antiparallel beta sheet, with the two strands connected at either end by tight turns (Fig. 2). Residues Leu^{10}, D-Phe^1, Pro^2, and Phe^3 form a type II beta turn, while at the other end of the molecule residues Asn^5, Gln^6, Tyr^7, and Val^8 form a slightly distorted type I beta turn (backbone dihedral angles are given in Table S1, Supplementary data). The two strands are connected by three hydrogen bonds between backbone amide and carbonyl groups (see Table 2). A fourth hydrogen bond is formed between the backbone amide of Val^8 and the side chain of Asn^5. The strand–strand association within the monomer is also stabilized by hydrophobic interactions between the side chains of D-Phe^4, Val^8, and Leu^{10}.

The arrangement of L- and D-amino acids in the tyrocidine sequence places more amino acid side chains on one face of the beta sheet than the other, giving rise to a pronounced curvature. Side chains oriented toward the convex face of the molecule include those of Phe^3, D-Phe^4, Asn^5, Tyr^7, Val^8, and Leu^{10}; in contrast, only the side chain of Orn^9 is found on the concave side of the sheet. The side chains of D-Phe^1 and Gln^6 protrude from either end of the molecule in an equatorial orientation.

The crystal asymmetric unit contains one tyrocidine monomer; however, in the crystal lattice each tyrocidine monomer associates with another monomer to form an intimate dimer, the two halves of which are related by a two-fold axis of symmetry. The curved beta sheets of each monomer pack edge-on, to form a continuous four-stranded antiparallel sheet, with four backbone–backbone hydrogen bonds joining the two monomers (Table 2). In addition, the dimer is stabilized by hydrophobic interactions between the side chains of Val^8 of one monomer and Leu^{10} of the opposite monomer. Further stabilization

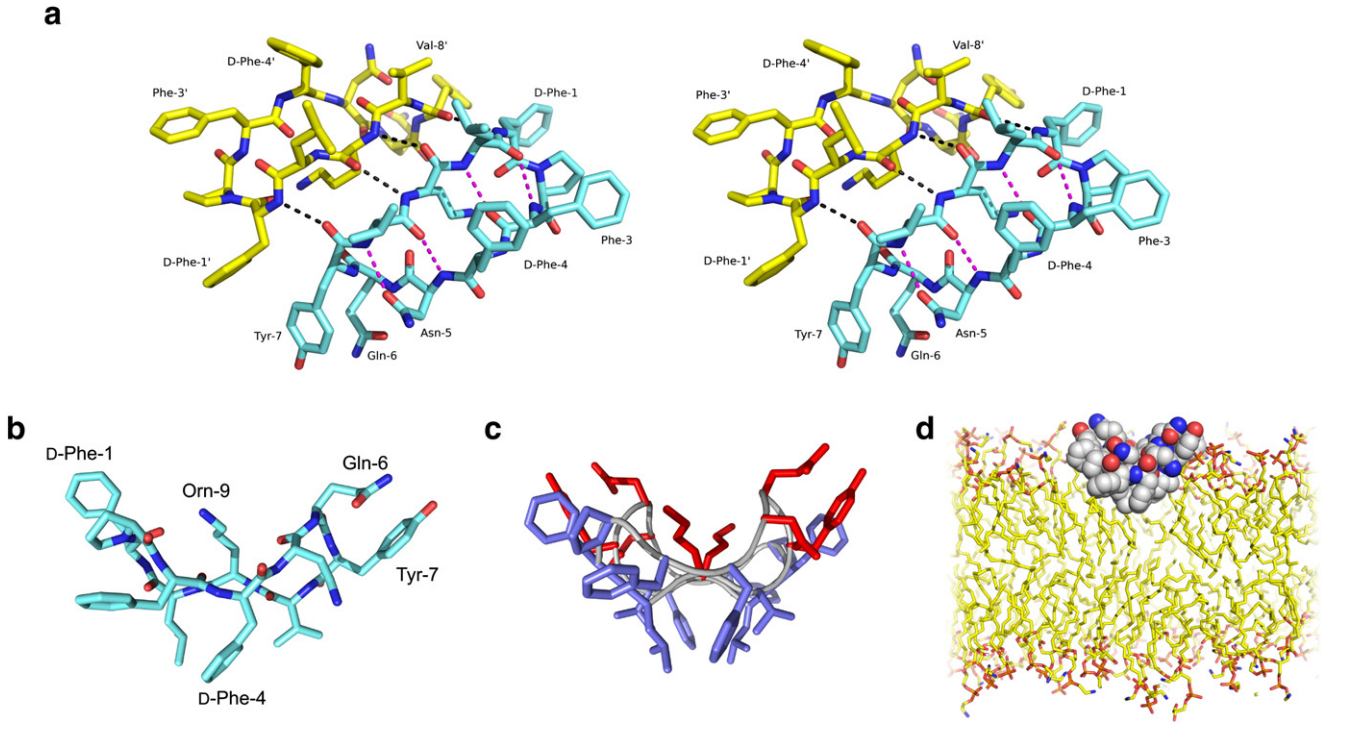

Fig. 2. The three-dimensional structure of tyrocidine A. (a) Stereoview of the tyrocidine A dimer. One monomer is colored cyan, and other yellow; oxygen atoms are colored red, and nitrogen atoms blue. Inter-subunit hydrogen bonds are shown as black dotted lines, while intra-subunit hydrogen bonds are shown in magenta. Selected residues are labeled. Shown is a glancing view of the convex (apolar) face of the dimer. (b) Side view of one tyrocidine monomer, showing the molecule's pronounced curvature. (c) Same view as in (b), showing the tyrocidine dimer. The color scheme has been chosen to highlight the amphipathic character of the dimer. For both monomers, the peptide backbone is shown in gray; hydrophobic side chains are shown in blue, while hydrophilic side chains are shown in red. (d) Speculative model for how the tyrocidine dimer interacts with membranes. The dimer is shown in a space-filling representation, in approximately the same orientation as seen in panel (c), with the apolar convex face inserting into the bilayer, and the polar concave face sitting at the level of the lipid head groups. In the antibiotic, carbon atoms are colored gray, oxygen atoms red, and nitrogen atoms blue. Carbon tails of the membrane lipids are shown in yellow, while head group oxygen, nitrogen, and phosphorous atoms are colored red, blue, and orange, respectively. Model lipid coordinates were taken from Pandit and Klauda [57].

is contributed by an edge-to-face interaction between the aromatic rings of D-Phe[1] and Tyr[7] on opposing monomers.

The interaction between the two halves of the dimer is considerably more extensive than any other crystal contacts. The surface area buried in the dimer interface is 264 Å^2, corresponding to 21% of the monomer's total surface area. The fraction of fully buried atoms in the dimer interface (f_{bu}) is 0.31, consistent with this interface representing a specific and biologically relevant recognition surface, rather than a fortuitous crystal contact [46].

The tyrocidine dimer structure is distinctly amphipathic. All of the amino acid side chains displayed on the convex face of dimer are hydrophobic, with the exception of the neutral polar Asn[5], which is engaged in a hydrogen bond with the backbone of the facing strand. In contrast, the only side chain found on the concave face of the molecule is that of the single charged residue, Orn[9]. In addition, backbone carbonyl oxygens of three residues that are not involved in strand–strand hydrogen bonds (D-Phe[1], Asn[5], and Gln[6]) point outward from the concave portion of the molecular surface; further, the side chain of Gln[6], which in the crystal structure extends equatorially to engage in a lattice contact, is well-positioned to turn toward the concave face as well. Hence, the concave face of the dimer adopts a polar character, while the opposite face is strongly apolar.

3.3. Tyrocidine interaction with membranes

Tyrocidine is known to disrupt membranes [13], but the details of the antibiotic–membrane interaction are lacking. To probe the nature of this interaction, we used surface plasmon resonance to directly assess tyrocidine binding to immobilized membranes. Using a lipid composition intended to mimic that of bacterial membranes, we found that tyrocidine bound readily and avidly to our immobilized membranes. The kinetics of the interaction proved complex, and were not adequately described by simple models such as reversible monomer or dimer binding or two-step binding processes. However, by using the conservative approach of plotting peak response values versus antibiotic concentration, we obtained an estimate for the overall apparent dissociation constant K_D of 9.7 μM (see Fig. 3a). To provide context, we note that the range of IC_{50} or minimum inhibitory concentration (MIC) values reported for tyrocidine A extends from 1 to 25 μM [18,19,21–23].

Next, to confirm that tyrocidine's membrane binding was linked to its membrane disruption properties, we examined the antibiotic's ability to permeabilize bacterial membranes, using an efflux assay in which drug-induced release of potassium ions from bacteria is measured with a potassium-sensitive fluorophore [42]. Using *M. luteus* as a model bacterial organism, we saw clear dose-dependent membrane disruption within the concentration range tested (0.8 to 8 μM), with an estimated EC_{50} value of 2.4 ± 0.9 μM (see Fig. 3b). Hence, tyrocidine binds tightly to membranes, and this binding correlates well with membrane disruption.

3.4. Tyrocidine orientation on membranes

The amphipathic structure of the tyrocidine dimer suggests a model for how the molecule might interact with membranes. In this model, the hydrophobic convex face would insert into the membrane, facing the bilayer interior, while the polar concave face would be oriented toward the aqueous phase (see Figs. 2d and 4a). To test this model, we prepared two variants of tyrocidine A, within which either a tyrosine or phenylalanine residue was replaced by the small intrinsic fluorescent probe *p*-cyanophenylalanine (*p*-CN-Phe) [47]. The two residues chosen for replacement were D-Phe[4] and L-Tyr[7], which were replaced by D- and L-*p*-CN-Phe, respectively. The side chain of D-Phe[4] extends from the center of the convex, hydrophobic face of the molecule, while Tyr[7] is at one end of the monomer, with the side chain oriented toward the concave, polar face of the molecule. Hence, in our simple model of membrane

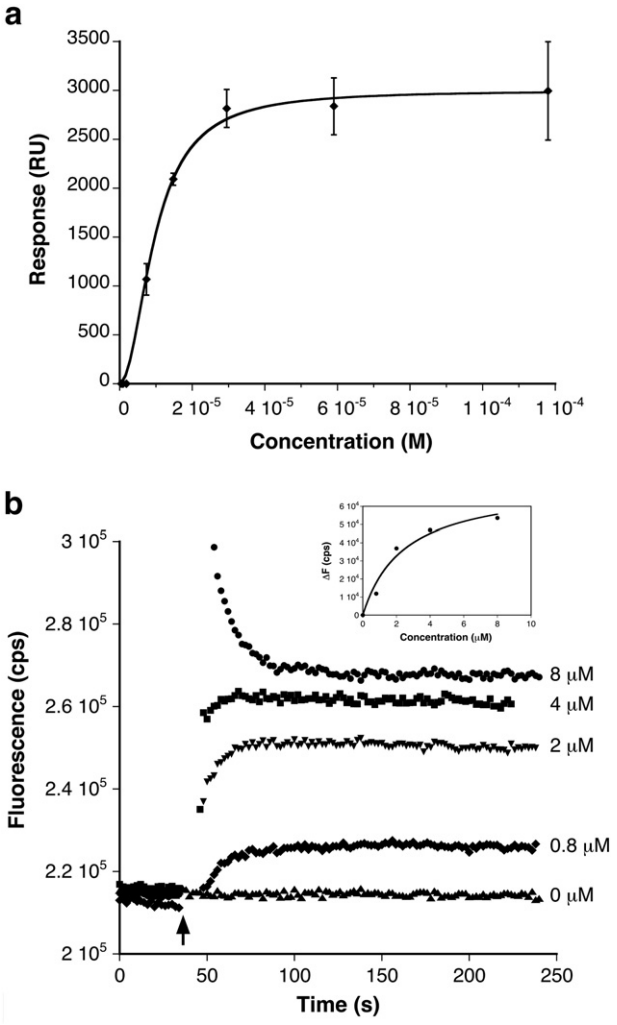

Fig. 3. Interaction of tyrocidine A with lipid membranes. (a) Binding of tyrocidine A to immobilized membranes, as monitored by surface plasmon resonance. (b) Permeabilization of bacterial membranes by tyrocidine A. Potassium release was monitored from *M. luteus* cells using the potassium-sensitive dye PBFI. Varying concentrations of the antibiotic were added at the time indicated by the arrow. The spike in fluorescence seen with 8 μM antibiotic likely represents transient local increases in [K^+] resulting from rapid catastrophic membrane depolarization. *Inset* shows the equilibrium change in fluorescence as a function of antibiotic concentration.

interaction, D-Phe[4] is predicted to be buried in the membrane interior, while Tyr[7] should be more solvent-exposed.

The solvent exposure of these two residues was first probed using hydrophilic quenchers of the *p*-CN-Phe fluorescence. In the absence of liposomes, the fluorescence of the probe at both the 4- and 7-positions was effectively quenched by both iodide and acrylamide (see Fig. S2, Supplementary data). The addition of liposomes at a 100:1 mole ratio of lipid to tyrocidine provided significant protection for both the [*p*-CN-Phe[4]] and [*p*-CN-Phe[7]] variants of the molecule, consistent with tyrocidine binding to the liposomes. Stern–Vollmer analysis was used to quantify the degree of protection afforded by membrane binding (Fig. 4). For both iodide and acrylamide, larger quenching constants were obtained when the *p*-CN-Phe probe was located at the 7-position, rather than the 4-position (Table 3), indicating a greater degree of protection for the probe located at the 4-position. Thus, the results with the soluble quenchers suggest that in the presence of membranes, tyrocidine's 7-position is more solvent-exposed than the 4-position.

We then turned to quenchers located within the membrane bilayer. We prepared liposomes containing phospholipids with dibrominated

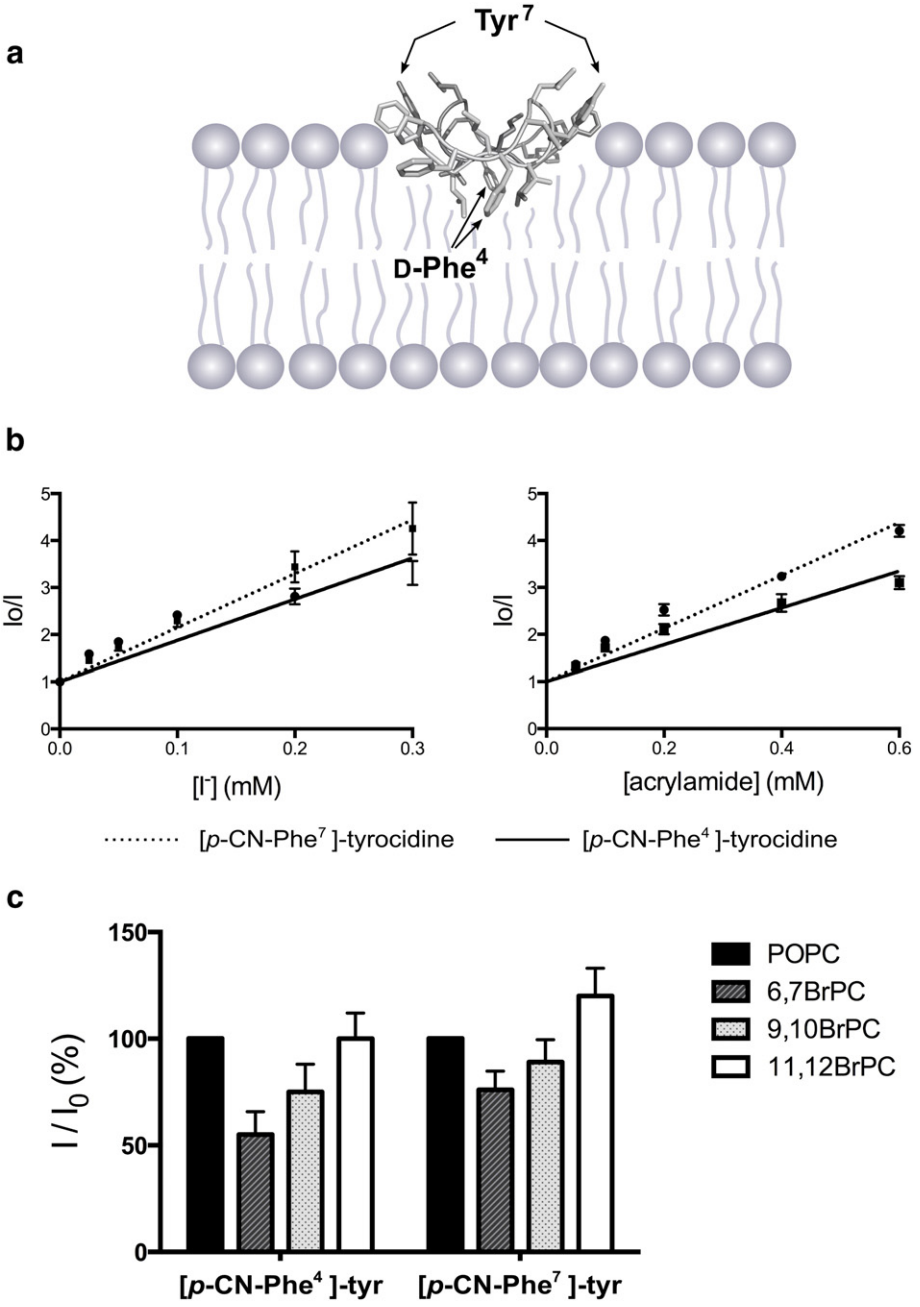

Fig. 4. Probing tyrocidine's interaction with membranes using fluorescence quenching. (a) Schematic model for the interaction of the tyrocidine dimer with membranes. The positions of the two residues labeled with the *p*-cyanophenylalanine probe are indicated. (b) Stern–Vollmer plots showing the quenching of labeled tyrocidine by iodide (left) and acrylamide (right), in the presence of liposomes. Data points represent the mean ± standard deviation from 3–5 replicates. Solid lines correspond to [*p*-CN-Phe^4]-tyrocidine and dashed lines to [*p*-CN-Phe^7]-tyrocidine. (c) Quenching of labeled tyrocidine by brominated phospholipids. Shown is the relative fluorescence of the labeled tyrocidine, as compared to the level observed in unbrominated POPC vesicles.

fatty acyl chains, in which the bromine atoms were inserted at either the 6–7, 9–10, or 11–12 positions. We then measured quenching of the two fluorescent tyrocidine variants for each type of liposome (Fig. 4). In each case, we observed that [*p*-CN-Phe^4]-tyrocidine was quenched more efficiently than [*p*-CN-Phe^7]-tyrocidine. Further, as the position of the quencher was moved deeper into the interior of the bilayer, quenching efficiency decreased monotonically for both the 4- and 7-labeled tyrocidine variants. These results indicate that the tyrocidine molecule is located near the membrane surface, with its 7-position being farther from the membrane interior than the 4-position.

Table 3
Stern–Vollmer quenching constants for 4- and 7-*p*-CN-Phe-tyrocidines.

Tyrocidine variant	Stern–Vollmer constant, iodide quenching (mM^{-1})[a]	Stern–Vollmer constant, acrylamide quenching (mM^{-1})[a]
[*p*-CN-Phe^4]	8.8 ± 0.6	3.9 ± 0.2
[*p*-CN-Phe^7]	11.5 ± 0.7	5.6 ± 0.2

[a] Values represent the mean ± standard deviation of 3–5 measurements.

4. Discussion

Tyrocidine was one of the first antibiotics to be discovered, and in the approximately sixty years since its discovery it has been studied extensively as a model for membrane-active natural products. Recently, tyrocidine and related cyclic decapeptides have become the objects of

renewed interest as the search for novel antibacterial agents has intensified [19,21,23]. Therefore, the structure of this molecule has been a topic of great interest. Initial NMR experiments provided an overall view of the molecule's conformation [31–34]; while the level of detail obtainable from such analyses does not approach that of a high-resolution crystal structure, the early NMR work allowed the inference of backbone torsion angles that are in essential agreement with the crystal structure and the prediction of three of the four intramolecular hydrogen bonds that link the two antiparallel strands (the fourth hydrogen bond, involving the side chain of Asn^5, was not correctly predicted from the NMR work, which instead posited the carbonyl oxygen of Asn^5 as the hydrogen-bond acceptor). More recently, NMR restraints have been incorporated into molecular dynamics simulations (NMR-MD) to obtain models for tyrocidine [48]; this work suggests that a hydrogen bond involving the carbonyl oxygen of Asn^5 is substantially less likely than the other three hydrogen bonds, in agreement with the crystal structure. Backbone phi/psi angles predicted by the NMR-MD method are also in good agreement with those seen in the crystal structure, with the notable exception of D-Phe^4. The NMR-MD phi/psi values for this residue (~180°/180°) lie at the edge of the allowed region in the Ramachandran plot, whereas the phi/psi values in the crystal structure lie well within the preferred region for D-amino acids (Table S1, Supplementary data). This difference has important structural ramifications, as the NMR-MD models place the side chain of D-Phe^4 facing the hydrophilic face of the molecule, whereas the crystal structure shows that it faces the opposite (hydrophobic) face. This leads the NMR-MD work to predict a substantially less amphipathic structure than what is revealed by the crystal structure. Because of the flipping of D-Phe^4, the NMR-MD models also fail to predict the marked curvature that is seen in the crystal structure. A similar flipped orientation was assigned to D-Phe^4 in another molecular modeling study [19]. Thus, this crystal structure should prove a valuable addition to the field, extending as it does the level of detail available from previous experimental structural work, as well as providing an objective standard against which future computational studies can be benchmarked.

In addition to providing a detailed view of tyrocidine's molecular architecture, this new structure also reveals a putative dimerization mode for the molecule. This dimerization has not been explicitly described in previous structural studies, although the molecule's propensity for self-association has been noted [12], and dimerization has been experimentally observed in an aqueous solution using mass spectrometry [48]. We speculate that the dimer seen in the crystal structure may be physiologically relevant, based both upon the significant molecular surface buried in the intimate dimer interface, and also upon the fact that the two monomers in the dimer associate in such as way as to preserve and amplify the amphipathic nature of the monomers. Further, the structure of the amphipathic dimer suggests a model for how tyrocidine interacts with bacterial target membranes (Fig. 4), which is consistent with the results of our fluorescence quenching experiments.

The advent of this crystal structure presents the opportunity to rationalize structure–activity data that have been accumulated for tyrocidine. In particular, we sought to explain these data in terms of both the molecule's three-dimensional structure and the membrane interaction model it suggests. Many structure–activity experiments have focused on specific positions in the molecule's peptide sequence, with two of the most intensively studied sites being D-Phe^4 and Gln^6. Substitutions at these positions significantly affect the therapeutic ratio (i.e., the ratio of the minimum hemolytic concentration to the minimum concentration required to inhibit bacterial growth) [18,21,24].

The structure reveals that D-Phe^4 lies in the center of the hydrophobic face of the tyrocidine dimer (Fig. 2), and our membrane interaction model predicts that the side chain of this residue penetrates into the hydrophobic core of the lipid bilayer. It is therefore not surprising that many different hydrophobic D-amino acids can be substituted at this position with little effect on the molecule's antimicrobial activity [18,21]. However, placing basic D-amino acids at this position sharply reduces antibacterial potency [18,19,23], consistent with the structural prediction that such substitutions should reduce amphipathicity and perturb membrane interactions. The retention of residual activity by such variants may reflect the fact that basic side chains are typically long and flexible (e.g., Lys or Arg), and can therefore "snorkel" around the side of the tyrocidine molecule to point toward the dimer's polar face [49]. In contrast, changing D-Phe^4 to basic L-amino acids results in molecules that retain antibiotic activity [18]. Such a D-to-L change would reverse the orientation of the residue's side chain, causing it to point toward the opposite side of the beta strand. Therefore, basic L-amino acids at position 4 would have their side chains oriented toward the molecule's basic face, reinforcing rather than reducing the molecule's amphipathic character. Interestingly, introducing N-methyl-D-Phe at position 4 does not compromise antibacterial activity [18], even though, in general, incorporation of N-methylated amino acids is not well tolerated by tyrocidine [23]. This general sensitivity to N-methylation likely reflects the importance of inter-strand hydrogen bonding. However, the backbone amide of residue 4 points outward from the edge of the dimer; it does not hydrogen bond with any other strands, either within the molecule or across the dimer interface, explaining why methylation at this particular position is tolerated.

Gln^6 lies in one of the beta turns connecting the two strands of the tyrocidine molecule. Gln^6 extends in an equatorial direction, midway between the molecule's polar and apolar faces (Fig. 2). In the crystal structure, the residue's side chain accepts a hydrogen bond from its own backbone amide nitrogen, and donates a second hydrogen bond to a symmetry-related molecule in the lattice. Of fourteen different L-amino acids that were substituted for Gln at this position, all were found to improve antibacterial activity except Glu, which gave equivalent activity to the parent compound [21]. A surprisingly diverse range of residues are tolerated at this position, including large hydrophobes such as leucine and tryptophan, uncharged polar amino acids such as serine, and both acidic and basic residues. Our membrane interaction model offers an explanation for how these disparate side chains can all function at the same position, predicting that the turn containing Gln^6 will lie at the interface between the hydrophobic interior of the bilayer and the lipid head groups. This interfacial location allows different types of side chains to be accommodated at position 6: polar side chains placed at this position can turn toward the polar face of the molecule, while hydrophobic side chains can turn in the opposite direction. These adjustments can be accomplished with small changes in dihedral angles and/or small changes in the overall orientation of the molecule.

Tyrocidine is closely related to gramicidin S, another cyclic decapeptide produced by *B. brevis*, and it is instructive to compare the structures of the two molecules. Crystal structures are available for gramicidin S itself [50,51], as well as for several chemically modified forms [52,53]. The most striking difference between tyrocidine and any of the gramicidin S structures is the difference in curvature, with tyrocidine being much more highly curved than any of the gramicidin structures (Fig. 5). This can be explained by the presence of two ornithine residues on the hydrophilic face of gramicidin S, as compared to the single ornithine found on tyrocidine's polar face. The extra positive charge and steric bulk contributed by the second ornithine is sufficient to prevent the two beta strands in gramicidin S from curling toward their hydrophilic face, resulting in a rather flat structure.

None of the gramicidin S crystal structures give any indication that the molecule forms a symmetric dimer analogous to that seen in the tyrocidine crystal structure. However, in certain of the gramicidin S crystal, forms infinite extended sheets are observed, wherein one molecule hydrogen bonds with a two-fold related neighbor, which in turn hydrogen bonds to another two-fold related neighbor, etc. [52]. This extended sheet formation is facilitated by the relatively flat shape of the gramicidin S monomer. In contrast, the more highly curved tyrocidine molecule exhibits a strong degree of twist within the two beta strands of the monomer; the two-fold related molecule twists in the opposite

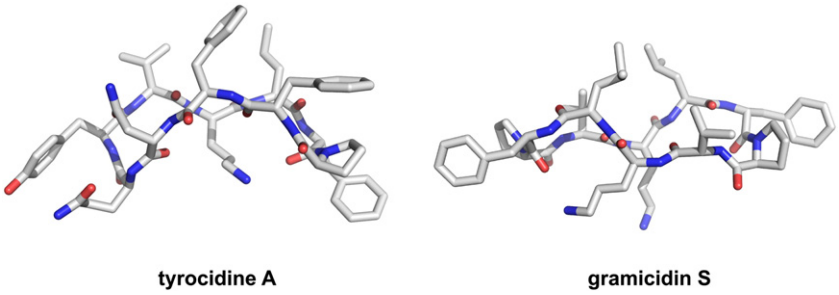

Fig. 5. Comparison of tyrocidine A and gramicidin S. A side view of both antibiotics is shown, emphasizing the difference in curvature.

direction, so while it is easy for two molecules to associate to form a dimer, linking these dimers into extended sheets is not feasible.

The significance of any higher order structure formation for antibiotic activity is not clear. It appears likely that tyrocidine will dimerize on target membranes, but it is much less clear that gramicidin S does so as well; yet both molecules effectively permeabilize membranes. Hence, it is possible that dimerization is not required for tyrocidine's permeabilization activity, but rather evolved to serve some other function. For example, tyrocidine binds and inactivates the linear peptide toxin gramicidin A [13], and interacts with RNA polymerase to inhibit initiation of transcription [54]; perhaps dimerization facilitates one of these roles. Alternatively, if assembly of higher order structures upon target membranes is required for permeabilization, perhaps gramicidin S accomplishes this by forming extended sheet structures, rather than the symmetric dimers favored by tyrocidine.

Interestingly, despite their structural differences, tyrocidine and gramicidin S appear to share similar modes of membrane interaction. Both experimental [55] and computational [56] studies agree that the amphipathic gramicidin S molecule localizes to the bilayer/water interface, with its two beta strands lying in the plane of the membrane and its hydrophobic side facing the bilayer core, in a manner essentially similar to what we propose for tyrocidine.

5. Conclusions

The atomic resolution structure of tyrocidine has now become known, revealing the precise details of the molecule's conformation and demonstrating the formation of an intimate and highly amphipathic dimer. This structure, together with supporting functional experiments, suggests a model for membrane interaction in which the dimer sits at the membrane–water interface, with the apolar convex face pointing downward into the membrane interior, and the polar concave face pointing upward toward the aqueous phase.

Acknowledgements

The authors gratefully acknowledge productive discussions with Paul Axelsen, and thank Irwin Chaiken and Rod Eckenhoff for access to equipment. We also thank Keven Owens for assistance with mass spectrometry. Model lipid coordinates for Fig. 2 were provided by Dr. J. Klauda at the Laboratory of Molecular and Thermodynamic Modeling at the University of Maryland. This research was supported in part by grant R01GM079508 (NIH/NIGMS). Diffraction data were collected at beamline X6A of the National Synchrotron Light Source. Financial support for NSLS beamlines comes principally from the Offices of Biological and Environmental Research and of Basic Energy Sciences of the US Department of Energy, and from the National Institute of General Medical Sciences of the National Institutes of Health.

Appendix A. Supplementary data

Supplementary data to this article can be found online at http://dx.doi.org/10.1016/j.bbamem.2014.01.033.

References

[1] G.L. French, The continuing crisis in antibiotic resistance, Int. J. Antimicrob. Agents 36 (Suppl. 3) (2010) S3–S7.
[2] M.A. Fischbach, C.T. Walsh, Antibiotics for emerging pathogens, Science 325 (2009) 1089–1093.
[3] R.J. Dubos, R.D. Hotchkiss, The production of bactericidal substances by aerobic sporulating bacilli, J. Exp. Med. 73 (1941) 629–640.
[4] R. Dubos, Tyrothricin, gramicidin, and tyrocidine—twenty years later, with remarks on the tissue factors which affect chemotherapy, Antibiot. Annu. 7 (1959) 343–349.
[5] H.L. Van Epps, Rene Dubos: unearthing antibiotics, J. Exp. Med. 203 (2006) 259.
[6] G.F. Gause, M.G. Brazhnikova, Gramicidin S and its use in the treatment of infected wounds, Nature 154 (1944) 703.
[7] K. Gebhardt, R. Pukall, H.P. Fiedler, Streptocidins A-D, novel cyclic decapeptide antibiotics produced by *Streptomyces* sp. Tu 6071. I. Taxonomy, fermentation, isolation and biological activities, J. Antibiot. (Tokyo) 54 (2001) 428–433.
[8] A. Holtzel, R.W. Jack, G.J. Nicholson, G. Jung, K. Gebhardt, H.P. Fiedler, R.D. Sussmuth, Streptocidins A-D, novel cyclic decapeptide antibiotics produced by *Streptomyces* sp. Tu 6071. II. Structure elucidation, J. Antibiot. (Tokyo) 54 (2001) 434–440.
[9] E. Katz, A.L. Demain, The peptide antibiotics of *Bacillus*: chemistry, biogenesis, and possible functions, Bacteriol. Rev. 41 (1977) 449–474.
[10] H. Kleinkauf, H. von Dohren, Nonribosomal biosynthesis of peptide antibiotics, Eur. J. Biochem. 192 (1990) 1–15.
[11] J.W. Trauger, R.M. Kohli, H.D. Mootz, M.A. Marahiel, C.T. Walsh, Peptide cyclization catalysed by the thioesterase domain of tyrocidine synthetase, Nature 407 (2000) 215–218.
[12] R.C. Williams, D.A. Yphantis, L.C. Craig, Noncovalent association of tyrocidine B, Biochemistry 11 (1972) 70–77.
[13] F.J. Aranda, B. de Kruijff, Interrelationships between tyrocidine and gramicidin A′ in their interaction with phospholipids in model membranes, Biochim. Biophys. Acta 937 (1988) 195–203.
[14] M.C. Goodall, Structural effects in the action of antibiotics on the ion permeability of lipid bilayers. 3. Gramicidins "A" and "S", and lipid specificity, Biochim. Biophys. Acta 219 (1970) 471–478.
[15] M.C. Goodall, Structural effects in the action of antibiotics on the ion permeability of lipid bilayers. I. Tyrocidine B, Biochim. Biophys. Acta 203 (1970) 28–33.
[16] M.C. Goodall, Structural effects in the action of antibiotics on the ion permeability of lipid bilayers. II. Kinetics of tyrocidine B, Biochim. Biophys. Acta 219 (1970) 28–36.
[17] S.H. Joo, Q. Xiao, Y. Ling, B. Gopishetty, D. Pei, High-throughput sequence determination of cyclic peptide library members by partial Edman degradation/mass spectrometry, J. Am. Chem. Soc. 128 (2006) 13000–13009.
[18] R.M. Kohli, C.T. Walsh, M.D. Burkart, Biomimetic synthesis and optimization of cyclic peptide antibiotics, Nature 418 (2002) 658–661.
[19] M.A. Marques, D.M. Citron, C.C. Wang, Development of Tyrocidine A analogues with improved antibacterial activity, Bioorg. Med. Chem. 15 (2007) 6667–6677.
[20] C. Qin, X. Bu, X. Wu, Z. Guo, A chemical approach to generate molecular diversity based on the scaffold of cyclic decapeptide antibiotic tyrocidine A, J. Comb. Chem. 5 (2003) 353–355.
[21] C. Qin, X. Zhong, X. Bu, N.L.J. Ng, Z. Guo, Dissociation of antibacterial and hemolytic activities of an amphipathic peptide antibiotic, J. Med. Chem. 46 (2003) 4830–4833.
[22] B.M. Spathelf, M. Rautenbach, Anti-listerial activity and structure–activity relationships of the six major tyrocidines, cyclic decapeptides from *Bacillus aneurinolyticus*, Bioorg. Med. Chem. 17 (2009) 5541–5548.
[23] Q. Xiao, D. Pei, High-throughput synthesis and screening of cyclic peptide antibiotics, J. Med. Chem. 50 (2007) 3132–3137.
[24] C. Qin, X. Bu, X. Zhong, N.L.J. Ng, Z. Guo, Optimization of antibacterial cyclic decapeptides, J. Comb. Chem. 6 (2004) 398–406.
[25] R.E. Hancock, Peptide antibiotics, Lancet 349 (1997) 418–422.
[26] V.G. Bulgakova, P.N. Korolev, G.I. Konoshenko, T. Novozhilova, A.N. Polin, Stability of *Escherichia coli* to the membranotropic antibiotic gramicidin S, Mikrobiologiia 59 (1990) 702–704.

[27] T.I. Orlova, V.G. Bulgakova, A.N. Polin, Cell wall components of gramicidin S resistant *Staphylococcus aureus*, Antibiot. Khimioter. 48 (2003) 13–17.
[28] T.I. Orlova, V.G. Bulgakova, A.N. Polin, V.A. Grushina, Cell wall components in *Staphylococcus aureus* with double resistance to gramicidin S and actinomycin D, Antibiot. Khimioter. 52 (2007) 3–8.
[29] M. Rautenbach, H.A. Eyeghe-Bickong, N.M. Vlok, M. Stander, A. de Beer, Direct surfactin–gramicidin S antagonism supports detoxification in mixed producer cultures of *Bacillus subtilis* and *Aneurinibacillus migulanus*, Microbiology 158 (2012) 3072–3082.
[30] D. Hodgkin, 50 years ago, Nature 438 (2005) 750.
[31] M. Kuo, W.A. Gibbons, Total assignments, including four aromatic residues, and sequence confirmation of the decapeptide tyrocidine A using difference double resonance. Qualitative nuclear overhauser effect criteria for beta turn and antiparallel beta-pleated sheet conformations, J. Biol. Chem. 254 (1979) 6278–6287.
[32] M.C. Kuo, W.A. Gibbons, Determination of individual side-chain conformations, tertiary conformations, and molecular topography of tyrocidine A from scalar coupling constants and chemical shifts, Biochemistry 18 (1979) 5855–5867.
[33] M.C. Kuo, W.A. Gibbons, Nuclear Overhauser effect and cross-relaxation rate determinations of dihedral and transannular interproton distances in the decapeptide tyrocidine A, Biophys. J. 32 (1980) 807–836.
[34] N. Zhou, P. Mascagni, W.A. Gibbons, N. Niccolai, C. Rossi, H. Wyssbrod, Confirmation of the solution structure of tyrocidine a using perturbation of proton relaxation rates by nitroxide spin labels, J. Chem. Soc. Perkin Trans. 2 (1985) 581.
[35] X. Bu, X. Wu, G. Xie, Z. Guo, Synthesis of tyrocidine A and its analogues by spontaneous cyclization in aqueous solution, Org. Lett. 4 (2002) 2893–2895.
[36] W. Kabsch, XDS, Acta Crystallogr. D Biol. Crystallogr. 66 (2010) 125–132.
[37] C.M. Weeks, R. Miller, The design and implementation of SnB v2.0, J. Appl. Crystallogr. 32 (1999) 120–124.
[38] P. Emsley, B. Lohkamp, W.G. Scott, K. Cowtan, Features and development of Coot, Acta Crystallogr. D Biol. Crystallogr. 66 (2010) 486–501.
[39] P.D. Adams, P.V. Afonine, G. Bunkoczi, V.B. Chen, I.W. Davis, N. Echols, J.J. Headd, L.W. Hung, G.J. Kapral, R.W. Grosse-Kunstleve, A.J. McCoy, N.W. Moriarty, R. Oeffner, R.J. Read, D.C. Richardson, J.S. Richardson, T.C. Terwilliger, P.H. Zwart, PHENIX: a comprehensive Python-based system for macromolecular structure solution, Acta Crystallogr. D Biol. Crystallogr. 66 (2010) 213–221.
[40] P.S.J. Chen, T.Y. Toribara, H. Warner, Microdetermination of phosphorus, Anal. Chem. 28 (1956) 1756–1758.
[41] Y.Q. Xiong, K. Mukhopadhyay, M.R. Yeaman, J. Adler-Moore, A.S. Bayer, Functional interrelationships between cell membrane and cell wall in antimicrobial peptide-mediated killing of *Staphylococcus aureus*, Antimicrob. Agents Chemother. 49 (2005) 3114–3121.
[42] T.J. Oman, W.A. van der Donk, Insights into the mode of action of the two-peptide lantibiotic haloduracin, ACS Chem. Biol. 4 (2009) 865–874.
[43] B. Magdoff-Fairchild, J.G. White, Tyrocidine A: crystal growth and preliminary X-ray diffraction data, J. Mol. Biol. 135 (1979) 757–760.
[44] R. Miller, G.T. DeTitta, R. Jones, D.A. Langs, C.M. Weeks, H.A. Hauptman, On the application of the minimal principle to solve unknown structures, Science 259 (1993) 1430–1433.
[45] I. Uson, G.M. Sheldrick, Advances in direct methods for protein crystallography, Curr. Opin. Struct. Biol. 9 (1999) 643–648.
[46] R.P. Bahadur, P. Chakrabarti, F. Rodier, J. Janin, A dissection of specific and non-specific protein–protein interfaces, J. Mol. Biol. 336 (2004) 943–955.
[47] A.L. Serrano, T. Troxler, M.J. Tucker, F. Gai, Photophysics of a fluorescent non-natural amino acid: *p*-cyanophenylalanine, Chem. Phys. Lett. 487 (2010) 303–306.
[48] G. Munyuki, G.E. Jackson, G.A. Venter, K.E. Kover, L. Szilagyi, M. Rautenbach, B.M. Spathelf, B. Bhattacharya, D. van der Spoel, beta-Sheet structures and dimer models of the two major tyrocidines, antimicrobial peptides from *Bacillus aneurinolyticus*, Biochemistry 52 (2013) 7798–7806.
[49] J.P. Segrest, H. De Loof, J.G. Dohlman, C.G. Brouillette, G.M. Anantharamaiah, Amphipathic helix motif: classes and properties, Proteins 8 (1990) 103–117.
[50] S.E. Hull, R. Karlsson, P. Main, M.M. Woolfson, E.J. Dodson, The crystal structure of a hydrated gramicidin S-urea complex, Nature 275 (1978) 206–207.
[51] G.N. Tishchenko, V.I. Andrianov, B.K. Vainstein, M.M. Woolfson, E. Dodson, Channels in the gramicidin S-with-urea structure and their possible relation to transmembrane ion transport, Acta Crystallogr. D Biol. Crystallogr. 53 (1997) 151–159.
[52] M. Doi, S. Fujita, Y. Katsuya, M. Sasaki, T. Taniguchi, H. Hasegawa, Antiparallel pleated beta-sheets observed in crystal structures of N, N-bis(trichloroacetyl) and N, N-bis(m-bromobenzoyl) gramicidin S, Arch. Biochem. Biophys. 395 (2001) 85–93.
[53] K. Yamada, M. Unno, K. Kobayashi, H. Oku, H. Yamamura, S. Araki, H. Matsumoto, R. Katakai, M. Kawai, Stereochemistry of protected ornithine side chains of gramicidin S derivatives: X-ray crystal structure of the bis-Boc-tetra-N-methyl derivative of gramicidin S, J. Am. Chem. Soc. 124 (2002) 12684–12688.
[54] H. Ristow, H. Paulus, Induction of sporulation in *Bacillus brevis*. 1. Biochemical events and modulation of RNA synthesis during induction by tyrocidine, Eur. J. Biochem. 129 (1982) 395–401.
[55] J. Salgado, S.L. Grage, L.H. Kondejewski, R.S. Hodges, R.N. McElhaney, A.S. Ulrich, Membrane-bound structure and alignment of the antimicrobial beta-sheet peptide gramicidin S derived from angular and distance constraints by solid state ^{19}F NMR, J. Biomol. NMR, 21, 2001, pp. 191–208.
[56] D. Mihailescu, J.C. Smith, Atomic detail peptide-membrane interactions: molecular dynamics simulation of gramicidin S in a DMPC bilayer, Biophys. J. 79 (2000) 1718–1730.
[57] K.R. Pandit, J.B. Klauda, Membrane models of *E. coli* containing cyclic moieties in the aliphatic lipid chain, Biochim. Biophys. Acta 1818 (2012) 1205–1210.